

Disappearing Wakes and Dispersion in Numerically Simulated Flows Through Tube Bundles

C. MOULINEC^{1,2}, J.C.R. HUNT^{1,3} and F.T.M. NIEUWSTADT¹

¹*J.M. Burgers Center, Laboratory of Aero and Hydrodynamics, Leeghwaterstraat 21, 2628 CA, Delft, The Netherlands; E-mail: f.nieuwstadt@wbmt.tudelft.nl*

²*Department of Mechanical Aerospace and Manufacturing Engineering, UMIST, Manchester M60 1QD, UK*

³*Departments of Space and Climate Physics and Geological Sciences, University College London, Gower*

Received 2 October 2003; accepted in revised form 11 February 2004

Abstract. Flow through a staggered array or 'bundle' of parallel rigid cylinders of diameter D is computed with the help of a three-dimensional direct numerical simulation (DNS) at various values of Reynolds number between 50 and 6000. Two different spacings L of the tubes, i.e. $L/D = 2$ and $L/D = 3$, have been considered. When $Re \lesssim 500$ the flow is laminar. In that case the converging flow between a pair of adjacent cylinders brings the oppositely signed vorticity at the two edges of the wake closer together behind the upstream cylinder so that the vorticity decreases quickly due to cancellation by diffusion. At $Re \approx 6000$, when the flow is highly turbulent, the wake vorticity disappears rather by turbulent diffusion. This 'disappearance' of the wakes in the closely packed flows (i.e. $L/D \lesssim 2$) causes the mean flow in a 'cell', which consists of the region around a single cylinder, to be effectively independent of that in other cells. Another consequence is that the mean velocity field can be very well approximated by potential flow except in a thin boundary layer along the cylinder and a short wake behind it. The results have been applied to the transport of scalars in closely packed arrays. As in other complex flows, the dispersion of the scalars is dominated by the divergence and convergence of the streamlines around the cylinder rather than by the wake turbulence. Approximate expressions are derived for this 'topologically' influenced dispersion in terms of the geometry of the array. The fact when most of the flow in the array can be approximated by a potential flow, allows us to introduce a fast approximate calculation method to compute the dispersion.

Key words: tube bundle, wake, direct numerical simulation, diagonal Cartesian method, potential flow

1. Introduction

The solution of many practical problems in fluid mechanics requires understanding of complex flows around groups of obstacles. Some well-known environmental problems involve the modelling of flow and diffusion around buildings, in crops and in forests. Industrial examples include the calculation of forces, heat and mass transfer around boiler tubes and around electronic components. Some examples of computations of the flow around tube bundles are for instance given by Planchard and Ibnou-Zahir [1], Schroder and Gelbe [2] and Longatte *et al.* [3]. The essential

feature of such complex flows is that the velocity field around any obstacle within the group is strongly affected by the presence of the adjacent obstacles. A generic configuration for this type of complex flow is the multiple connected flow region consisting of a regular array of rigid cylinders. The mean flow in a plane perpendicular to the cylinders is two-dimensional. Even for this relatively 'simple' geometry the flow is poorly understood.

Some of the interesting questions about this flow geometry, which have a generality even for three-dimensional flows [4], can be formulated as follows. Is there significant repeatability of the flow in the array and therefore is it a good approximation to compute the average properties of the array by only computing the flow over one 'wavelength' or 'cycle' of the array? If this is indeed the case, what is the 'wavelength' or 'repetition length' in terms of the distance between obstacles? (For example, are one or two spacings sufficient?) How do such approximations vary with the Reynolds number and the relative spacing of the obstacles? How does the flow structure vary around a cylinder in the array and what is the effect on scalar diffusion? Is the flow sufficiently insensitive to the precise shape of the obstacle so that calculations can be sped up by not satisfying the boundary condition on the obstacle exactly? When is potential flow a useful approximation for flow around groups of obstacles? Such an approximation may be justified when wake vorticity in the flow within closely packed bluff bodies disappears as a result of converging streamlines. In that case the cancellation of the vorticity of opposite sign in the wake is accelerated by cross diffusion [5]. This process of cross diffusion largely determines the extent and strength of wakes of cylinders in closely packed arrays and therefore the repetition 'wavelength' L_C of the flow in the array. The approximation by potential flow is especially useful for estimating dispersion of scalars. For instance, Davidson *et al.* [6] showed that calculation of diffusion from line sources placed within an array of cylinders, in which the flow was based on potential theory, corresponded quite closely with measurements at finite Reynolds numbers.

At high Reynolds numbers the interaction between the turbulence and the flow distortion around the obstacles affects the wake eddies, firstly by the straining of these eddies through mechanisms studied in idealized flows by Elliot and Townsend [7]. The spreading of the wake may or may not be enhanced depending on the balance between converging streamlines and distortion of turbulence [8]. Secondly, the wake eddies are affected by the blocking distortion as they impact on downstream cylinders [9], leading to increased fluctuating pressures, heat transfer and noise [10].

In the previous work of Benhamadouche and Laurence [11], Rollet-Miet *et al.* [12], Bouris and Bergeles [13] and Hassan and Ibrahim [14] it has become clear that the essentially non-stationary flow in tube bundles can only be computed properly by means of numerical simulations. Computations based on the Reynolds-averaged equations are not sufficient because these have been found to underpredict turbulence quantities and recirculation lengths. Therefore, we turn in the present study

to a numerical simulation of the flow in a regular array of cylinders. By varying the spacing of the cylinders, the repetition 'wavelength' is estimated. Some of the mechanisms and phenomena discussed above are identified. This study should help in the practical application of numerical methods to tube arrays and to comparable complex geometries. We present results of computations carried out both at low Reynolds numbers, where the flow is laminar at first steady two-dimensional and progressing to unsteady three-dimensional, and at high Reynolds numbers, where the flow is turbulent. In the latter case the effective Reynolds number of the simulations considered is sufficient to study the broad distortion effects on the energy containing eddies, but it is not high enough for studying the fine detail of the turbulence structure. As an application of this complex flow we also use the numerical simulation results to investigate diffusion of a scalar within a tube bundle. The results are compared with those obtained for isolated cylinders and with the concept of 'topological' diffusion proposed by Davidson *et al.* [6].

2. Problem Definition and Numerical Procedure

2.1. DESCRIPTION OF THE TUBE BUNDLE CONFIGURATION

Let us consider a staggered tube bundle with the tube axes perpendicular to the x - y plane as illustrated in Figure 1. The cylindrical tubes have an infinite length in the spanwise z -direction. The distance between two neighbouring tubes is taken equal both in the vertical and horizontal direction. The mean flow through the bundle is directed along the x -axis.

2.2. NUMERICAL PROCEDURE

In our numerical procedure we solve the incompressible three-dimensional Navier-Stokes equations, which read in their conservative form:

$$\begin{aligned} \frac{\partial \mathbf{u}}{\partial t} + \nabla \cdot (\mathbf{u}\mathbf{u}) &= -\frac{1}{\rho} \nabla p + \nabla \cdot \{\nu(\nabla \mathbf{u} + \nabla^T \mathbf{u})\} + \mathbf{f} \\ \nabla \cdot \mathbf{u} &= 0 \end{aligned} \quad (1)$$

where \mathbf{u} is the velocity such that $\mathbf{u} = (u, v, w)^T$, p the pressure, t the time, ρ the density and ν the kinematic viscosity. The equations are discretized by the finite volume method [15]. In this method the variables are defined on a Cartesian mesh in a staggered arrangement with the pressure in the centre of a grid volume and the velocity components on the sides. To allow for non-rectangular boundaries the diagonal Cartesian method [16,17] is used. In this method the physical boundaries of the cylinder, which do not fit on the rectangular Cartesian mesh, are approximated by means of the cell sides and the diagonals of the rectangular cells.

The projection method [18,19] is employed to solve the velocity-pressure coupling. The first step of this method gives a prediction of the velocity field by solving the momentum equation without the pressure term. This predicted velocity field is

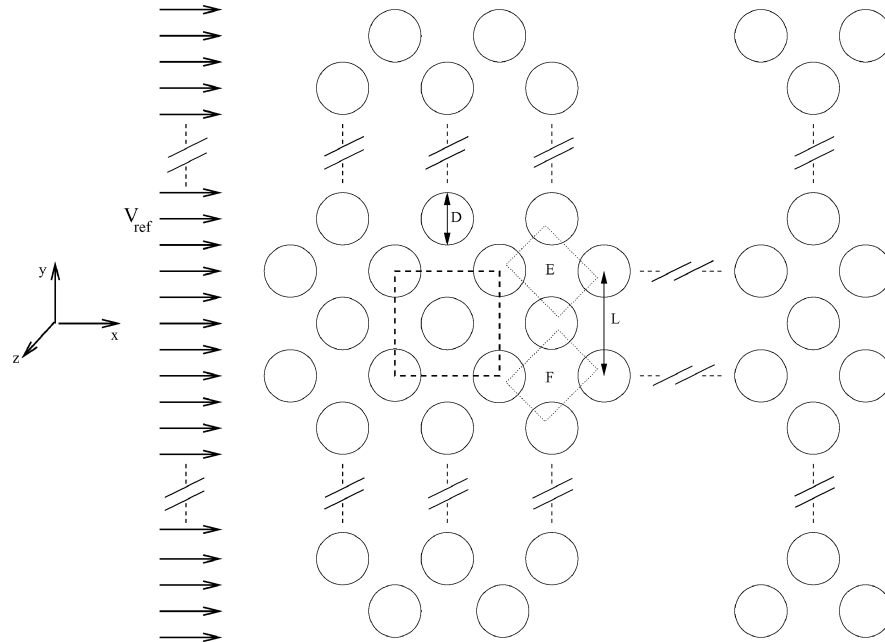


Figure 1. Staggered tube bundle (no side walls) consisting of an array of cylinders with diameter D and at a distance L between their centres. The rectangular region bounded by the dashed curve indicates an elemental computation cell. E and F correspond to the part of the geometry where the flow accelerates or the straining occurs, which are considered in section 6.

generally not divergence free. To ensure continuity this velocity field is corrected by a pressure gradient, which is obtained from the solution of a Poisson equation. This equation is solved by an iterative solver coupled with a fast Fourier transform in the homogeneous z -direction, which is in our case the direction parallel to the cylinders in the tube bundle.

The time discretization is performed by the Euler backward scheme for steady flows and by the Adams-Bashforth scheme otherwise. The convective terms are discretized by a second-order central difference scheme.

2.3. FLOW REGION AND BOUNDARY CONDITIONS

Depending on the distance between the tubes, the mean flow becomes periodic after a certain number of rows [20,21]. Periodicity in this case implies that the mean field and turbulence statistics are invariant for a linear translation over one tube distance in the x - y plane. The question then arises what should be the length L_C in the x - y plane where L_C is the size of the computational domain needed to compute the periodic flow field. In other words, how many tubes have to be embedded into this domain to get a realistic solution, which is independent of L_C . Furthermore, what kind of boundary conditions have to be applied and what should be the length of the computational domain in the z -direction?

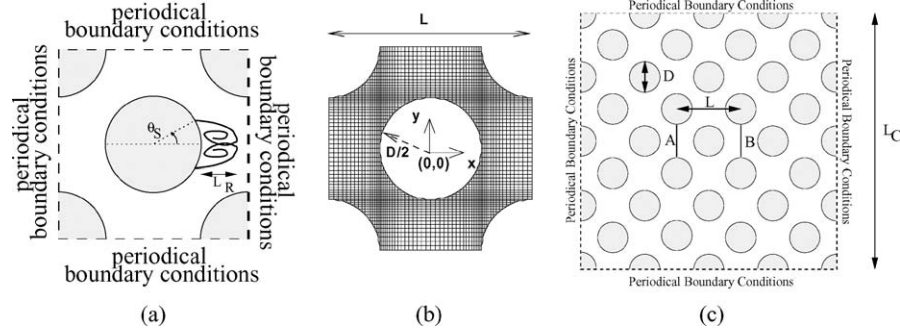


Figure 2. (a) 'Elemental cell', (b) mesh of an 'elemental cell' for the diagonal Cartesian method, (c) domain with 16 'elemental cells'.

The smallest size for the computational region is $L_C = L$, which is called an 'elemental cell'. It consists of one cylinder in its centre and four cylinder quarters in its corners as indicated by the dashed box in Figure 2(a) and which is also indicated by the region bounded by the dashed curve in Figure 1. Rollet-Miet *et al.* [12] show in their large-eddy simulations that an 'elemental cell' is sufficient as a computational domain. This choice for the computational region is also confirmed by the direct numerical simulation of Moulinec *et al.* [17]. Here, we shall also consider a second computational domain which consists of 16 'elemental cells' or $L_C = 4L$ as shown in Figure 2 (c). The latter is called the 'wide domain'. For both domains, periodic boundary conditions are applied.

The flow is driven by a mean pressure gradient in the x -direction, i.e. $\mathbf{f} = (f, 0, 0)$, which is adjusted at each time step to keep the mass flow constant. Both two- and three-dimensional computations have been carried out. For all three-dimensional computations the size of the computational region in the spanwise direction, i.e. parallel to the tubes has been taken equal to D . The boundary conditions in this direction are periodic.

We have carried out numerical simulations for various flow conditions, which are characterized in terms of the Reynolds number $Re = V_{\text{ref}} D / \nu$ where V_{ref} is the mean velocity in the x -direction in absence of the tube bundle (see Figure 1). For $0 < Re \lesssim 200$ the flow is laminar and two-dimensional. For $200 \lesssim Re < Re_t$ the flow becomes three-dimensional but it still can be considered as laminar. Beyond Re_t , the transition Reynolds number, the flow should be considered as fully turbulent and thus by definition three-dimensional. For our computations of the laminar flow field we have considered two spacings L between the tubes. In the first case, the distance L is equal to two diameters D ($L = 2D$) and for the second, we take $L = 3D$. For the case of two-dimensional flow and $L = 2D$ we use a mesh of 64×64 grid points to compute the flow in an 'elemental cell' and 256×256 grid points for the 'wide domain'. The mesh of 64×64 grid points is illustrated for this case in the Figure 2(b). For the case of two-dimensional flow and $L = 3D$ we

Table I. Number of grid points used in the various computations.

Re	$L \approx 2D$			$L = 3D$	
	$0 - 210$	$210 \lesssim Re \lesssim Re_t$	$Re = 6000$	$Re = 0 - 200$	$200 \lesssim Re \lesssim Re_t$
Dimension/flow	2-D/Lam	3-D/Lam	3-D/Turb	2-D/Lam	3-D/Turb
Elemental cell	64×64	$64 \times 64 \times 16$	$196 \times 196 \times 128$	96×96	$96 \times 96 \times 16$
Wide domain	256×256	$256 \times 256 \times 16$		384×384	

The Re_t represents the Reynolds for the transition between laminar and turbulent flows and has not been calculated in this study. ‘Lam’ stands for laminar flow and ‘Turb’ for turbulent flow.

have used 96×96 grid points for the ‘elemental cell’ and 384×384 grid points for the ‘wide domain’. For the case of three-dimensional laminar flow we have used $64 \times 64 \times 16$ grid points for the case $L = 2D$ and $96 \times 96 \times 16$ grid points for the case $L = 3D$. For the case $L = 2D$ computations were carried out for the ‘wide domain’ with $256 \times 256 \times 16$ grid points. For the fully turbulent case only the flow with $L = 2D$ has been considered in an ‘elemental cell’ with a resolution of $196 \times 196 \times 128$ grid points on a stretched mesh. The various resolutions used in the simulations have been summarized in Table I.

For the cases where we have carried out computations in the wide domain, we can check whether a domain consisting of an ‘elemental’ cell is sufficient for the computation of the flow field. To this end we have carried out a computation both for $L = 2D$ and $3D$ at $Re = 150$ where the flow is two-dimensional and unsteady and for $Re = 300$ where the flow is three-dimensional.

To check the validity of periodic boundary conditions for the ‘elemental cell’, we introduce two quantities $\Delta\epsilon_0$ and $\Delta\epsilon_1$, respectively, defined as $\Delta\epsilon_0 = \max_{(A,B)} |\epsilon_B - \epsilon_A|$ and $\Delta\epsilon_1 = \max_{(A,B)} |2(\epsilon_B - \epsilon_A)/(\epsilon_B + \epsilon_A)|$. The ϵ will be defined hereafter based on the fact whether the flow is two- or three-dimensional. The A and B are the locations where the two values of ϵ are computed and for these we choose the sections illustrated in Figure 2 (c).

For the cases that the flow is two-dimensional, i.e. at $Re = 150$, the ϵ is chosen equal to variables, u_x , which is the x -component of the velocity vector \mathbf{u} , and to p . For $L = 2D$, the order of magnitude of $\Delta\epsilon_0$ and $\Delta\epsilon_1$ is found to be 10^{-15} , which corresponds to the machine precision. For $L = 3D$, $\Delta\epsilon_0$ and $\Delta\epsilon_1$ are smaller than 10^{-11} . Such small values of $\Delta\epsilon_0$ and $\Delta\epsilon_1$ imply that the flow in the ‘elemental cell’ can indeed be considered as periodic. Therefore it is justified to use the ‘elemental cell’ with periodic boundary conditions as the computational domain for two-dimensional flows.

For the three-dimensional case, i.e. $Re = 300$, ϵ is now computed based on the variables \bar{U} , \bar{V} , which are the x - and y -components of the mean velocity vector averaged in time and in the z -direction, and the $\overline{u'^2}$, $\overline{v'^2}$ and $\overline{u'v'}$, which are the Reynolds stresses averaged in time and in the z -direction. After 180 s of computation which

Table II. Order of magnitude of $\Delta\epsilon_0$ and $\Delta\epsilon_1$ for the ‘wide cell’ at $Re = 300$ and $L = 2D$.

	\bar{U}	\bar{V}	$\overline{u'u'}$	$\overline{v'v'}$	$\overline{u'v'}$
ϵ_A	1.031	0.234	0.156	0.189	2.05e-02
ϵ_B	1.0281	0.233	0.155	0.188	2.13e-02
$\Delta\epsilon_0$	3.4e-03	1.2e-03	1.7e-03	9.6e-04	7.8e-04
$\Delta\epsilon_1$	3.31e-03	5.0e-03	1.1e-02	5.1e-03	3.7e-02

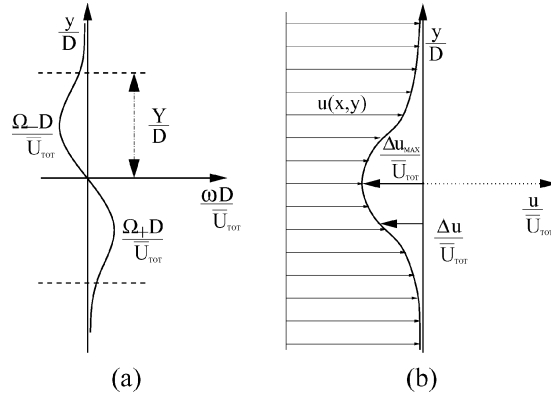


Figure 3. Wake flow past a single cylinder. (a) Vorticity profile, (b) velocity profile and definition of $\Delta u(x, y)$, the velocity defect.

represents around 35 crossings of the ‘wide domain’, $\Delta\epsilon_0$ becomes never bigger than 0.3% and $\Delta\epsilon_1$ never bigger than 3.7% (see Table II). Those values are considered small enough in regard to the coarseness of the grid that periodic boundary conditions can be assumed to be valid for the three-dimensional ‘elemental cell’, as long as one is only interested in the flow statistics.

3. Wake Flow Analysis

As mentioned above, for the case of two-dimensional laminar flow we have considered the tube-bundle for two cases $L = 2D$ and $3D$. In particular we investigate the wake behind the central cylinder in the ‘elemental cell’. The results can be compared with the theory developed by Hunt and Eames [5] on the wake behind a single cylinder in a planar straining flow.

A wake flow can be characterized by a number of dimensionless quantities. These are for instance the recirculation length L_R/D and the separation angle θ_S , which have the same interpretation for the case of the flow behind a single cylinder and the flow in the tube bundle and they are illustrated in Figure 2(a).

The two-dimensional wake flow can be further characterized by the profile of the vorticity component in the z -direction $\omega(x, y)$, which is illustrated in Figure 3(a) for the case of a single cylinder and in Figure 4(a) for the case of the tube bundle.

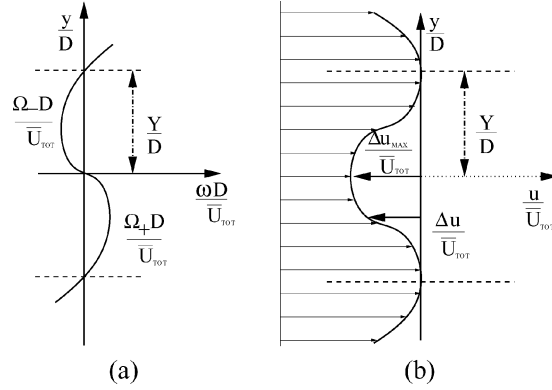


Figure 4. Wake flow in a tube bundle where $y = 0$ is the centreline. (a) Vorticity profile, (b) velocity profile and definition of $\Delta u(x, y)$, the velocity defect.

The vorticity is an anti-symmetric function of y and for the case of a single cylinder it goes to 0 for $y \rightarrow \infty$. For the case of the tube bundle, however, the vorticity changes sign as shown in Figure 4(a). This is due to the boundary layers that develop on the neighbouring cylinders.

Based on these vorticity profiles we define the maximum value of the vorticity Ω as $\Omega(x) = \frac{1}{2}(\Omega_+(x) - \Omega_-(x))$, where $\Omega_+(x)$ and $\Omega_-(x)$ are the maximum values of the positive and negative vorticity, respectively (see Figure 3(a) for the case of the single cylinder and Figure 4(a) for the tube bundle). To characterize the wake the following dimensionless parameter is introduced: $\Omega(x)D/\bar{U}$ where \bar{U} is the free-stream velocity $u(x, \infty)$ for the case of the single cylinder and $\bar{U} = V_{\text{ref}}$ for the case of the tube bundle.

Another parameter to characterize the wake flow is the width of the vorticity wake $Y(x)$. For the case of the single cylinder it is given by the distance from the centre line where the vorticity has dropped to a small value. For the case of the tube bundle we take $Y(x)$ as the distance from the centre line to the y -coordinate where the sign of $\omega(x, y)$ reverses as shown in Figure 4(a).

In addition to $\Omega(x)$ and $Y(x)$ also consider the volume flux $Q(x)/(\bar{U}D)$, which is defined as

$$Q(x) = - \int_{-Y(x)}^{+Y(x)} \Delta u(x, y) dy. \quad (2)$$

where $\Delta u(x, y)$ is the velocity defect illustrated in Figures 3(b) and 4(b). For the case of a wake behind a single cylinder the velocity defect can be interpreted as $\Delta u(x, y) = u(x, y) - u(x, \infty)$ and for the integral in Equation (2) the $Y(x)$ can be taken as $\rightarrow \infty$ as illustrated in Figure 3(b). For the tube bundle the definition of $Q(x)$ follows with $\Delta u(x, y) = u(x, y) - u(x)_{\text{max}}$ and $Y(x)$ as defined above.

Hunt and Eames [5] have studied the wake behind a single cylinder for the case of a uniform planar straining flow (with strain rate $\alpha > 0$) both for laminar and

Table III. Comparison of the evolution of the vorticity maximum and the volume flux in case for a constant non-straining flow and for laminar/turbulent straining flows of a wake behind a single obstacle in the asymptotic limit far from the obstacle

	Constant flow	Laminar straining flow	Turbulent straining flow
$\Omega(x)$	x^{-1}	x^{-2}	x^{-2}
$Q(x)$	x^0	x^{-2}	x^0

turbulent flow conditions. The results for $\Omega(x)$ and $Q(x)$ in the asymptotic limit $x \rightarrow \infty$ are given in Table III where they are compared with the results for the case of a constant non-straining flow. We see that when the flow is laminar the variation of Ω and Q with x is the same for both parameters in contrast with the results for the wake flow in a non-straining constant flow. The reason why Ω and Q have the same variation with x is due to the fact that far enough from the obstacle the wake reaches a constant thickness Y_∞ of order v/α so that:

$$\begin{aligned}\Omega(x) &\sim \frac{\Delta u_{\max}}{Y(x)} \sim \frac{\Delta u_{\max}}{Y_\infty} \\ Q(x) &\sim \Delta u_{\max} Y(x) \sim \Delta u_{\max} Y_\infty.\end{aligned}\quad (3)$$

For the case of a tube bundle, the wake behind each cylinder is perturbed by the presence of neighbouring tubes. Directly behind each cylinder the flow is converging and this perturbation is comparable to the influence of straining (with positive α). This means that the wake behind a cylinder in a tube bundle may be compared to the case of the straining flow behind a single obstacle as discussed above so that the wake should decay faster than for the case of a constant non-straining flow. This is the hypothesis that we will investigate with help of our numerical results in the next section.

The same analysis applies in a strained turbulent wake far from the body, provided ν is now taken to be the eddy viscosity [5]. If the turbulence is very strong or $\overline{v'^2} \sim \overline{u'^2}$, the wake diffuses like a passive scalar (e.g. Townsend, 1976). In that case the convergence effect is weak and we expect

$$\begin{aligned}Y(x) &\sim x \\ \Delta u_{\max} &\sim \frac{1}{x}.\end{aligned}\quad (4)$$

so that $\Omega(x) \sim 1/x^2$ while and $Q(x) \sim \Delta u_{\max} Y(x) \sim \text{constant}$.

4. Numerical Results

4.1. LAMINAR FLOW

Let us first consider the configuration with $L = 2D$. In Figure 5 we have plotted the maximum of vorticity Ω and volume flux Q as a function of x together with

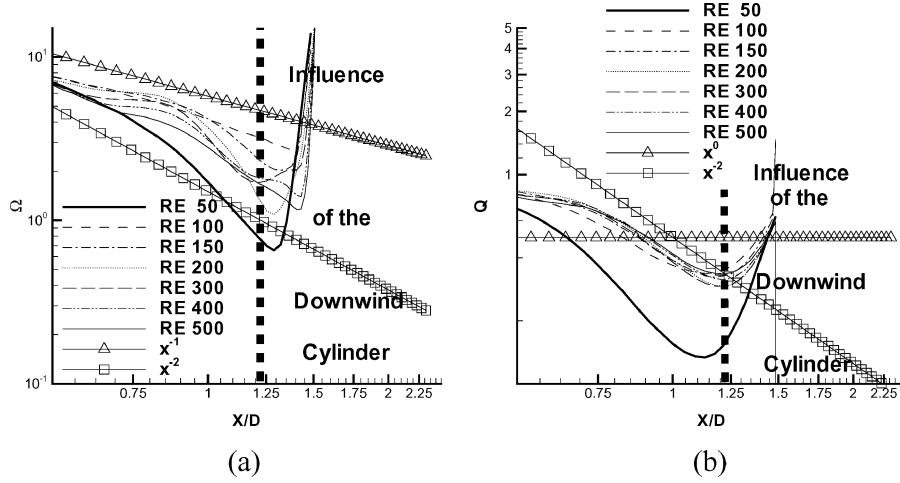


Figure 5. Wakes in a closely packed bundle ($L = 2D$). (a) Vorticity maximum along x -axis, (b) volume flux along x -axis. Symbols indicate the theoretical asymptotic slopes (see Table III): \triangle single cylinder in a constant flow, \square in a straining flow [5]. The thick dashed line indicates the boundary beyond which the influence of the downstream cylinder starts to be felt.

the theoretical relationships given in Table III for the various Reynolds numbers, for which computations have been carried out. For small to moderate Reynolds numbers ($Re = 50, 100$), the flow is steady and the slopes of the curves of the maximum vorticity in Figure 5(a) are almost straight, which implies a power law behaviour for the region starting after the recirculation zone and before the impact on the downstream cylinder. When $Re = 50$, the greater wake thickness means that the asymptotic theory is not valid, so that $Q(x)$ decays faster than x^{-2} (see Figure 5(b)). The behaviour for $Re = 100$ is closer to the results for the higher Reynolds number, for which the shear layers become thinner and the peak vorticity increases in accelerating the flow downwind of the cylinder ($0.5 < x/D < 1$). For $1 < x/D < 1.3$, the vorticity decreases rapidly when the ‘wake disappearing’ effect is the strongest. Concerning the volume flux the slope of $Q(x)$ at higher Reynolds number tends to behave like x^{-2} as in the theoretical prediction for laminar straining flows. Therefore, it seems that for the case of $L = 2D$, the wake behind a cylinder in a tube bundle has almost the same behaviour as in a straining flow.

It follows from the numerical simulations that the shedding appears around $Re = 125$ whereas for a single isolated cylinder in an unbounded uniform flow shedding appears at $Re = 40$. This big difference between the shedding Reynolds number for the isolated cylinder and the tube bundle, can be explained by the reduced scale of the wake in the latter case. Another transition in the wake flow occurs at $Re \approx 200$, when the flow in the tube bundle becomes three-dimensional (see Table I). This is approximately the same value as found for a single cylinder [22]. The average separation angle θ_S and the recirculation length L_R are shown in Figure 6 as a function of Re .

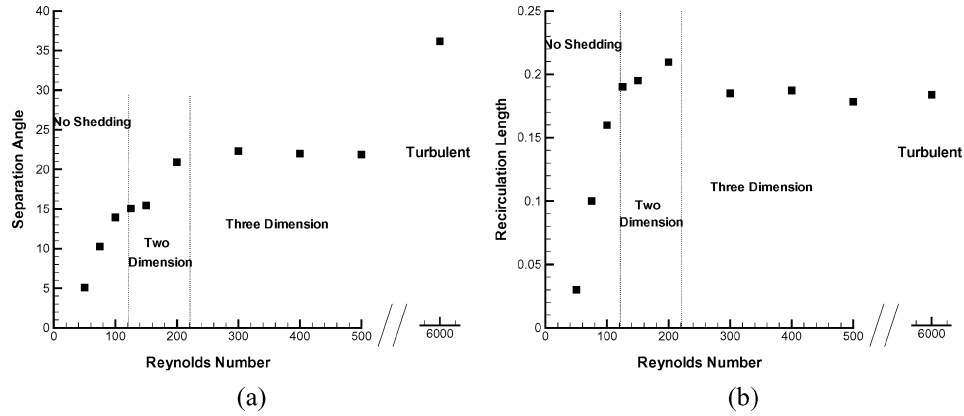


Figure 6. Wakes in a closely packed bundle ($L = 2D$). (a) Separation angle versus Reynolds number, (b) recirculation length vs. Reynolds number.

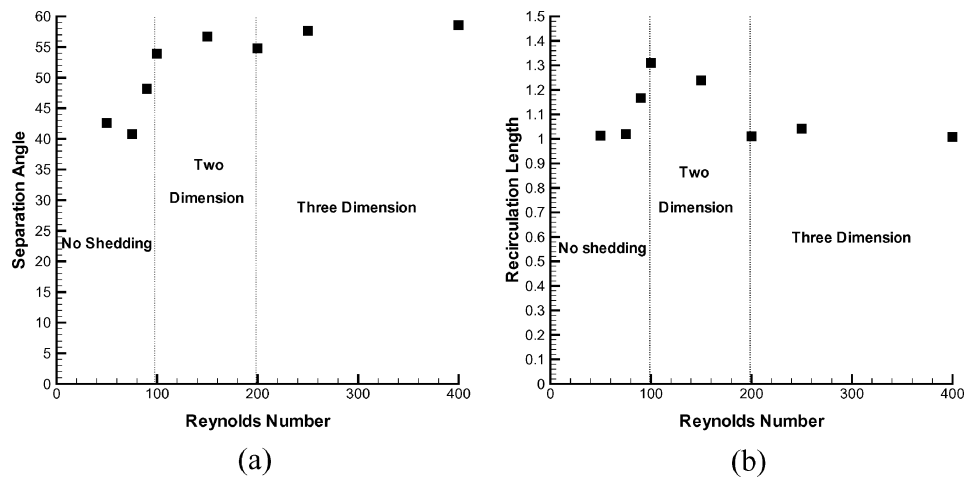


Figure 7. Laminar wakes, large spacing ($L = 3D$). (a) Separation angle/Reynolds number, (b) recirculation length/Reynolds number.

Next we consider a larger spacing between cylinders, i.e. $L = 3D$. The results for the separation angle θ_S and the recirculation length L_R are shown in Figure 7 as a function of the Reynolds number. The transition between steady and unsteady flows in this case appears just before $Re = 100$ and the flow becomes three-dimensional at $Re = 200$. Note that at $Re = 300$, it appears that no recirculation zone exists. For Re larger than 350, the recirculation zone reappears.

The variation of the vorticity maximum and the volume flux along x -axis is shown in Figure 8. For Reynolds numbers up to 200 the maximum of vorticity $\Omega(x)$ varies approximately in proportion to x^{-1} , which is the same as in a constant non-straining flow. However at higher Reynolds numbers the vorticity decays slightly faster as a result of the straining effect by the neighbouring tubes. The results for

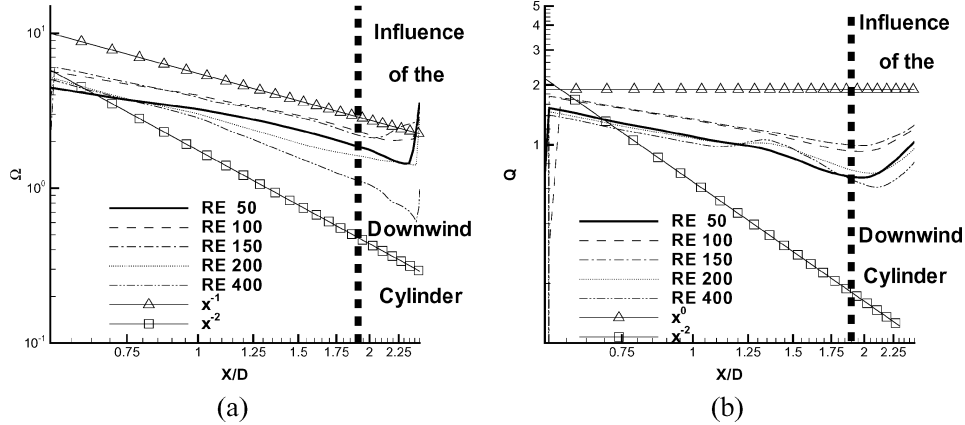


Figure 8. Laminar wakes, large spacing ($L = 3D$). (a) Vorticity maximum along x -axis. (b) volume flux along x -axis. Notation for the asymptotic slopes of theoretical curves is as in Figure 2 (b): Δ isolated cylinder (laminar/turbulent flow), \square in straining flow (following [5]).

$Q(x)$ shows also a mixed behaviour between the results for uniform and strained flow. The transition to three-dimensional flow at $Re = 200$ does not seem to greatly affect the evolution of $Q(x)$.

Comparison of these results for $L = 2D$ and $3D$ shows that for the case $L = 2D$ the wakes effectively ‘disappear’ so that except for the boundary layers near the cylinder and a small separation region much of the flow field can be regarded as a potential flow. For the case with the larger spacing where $L = 3D$, the wakes disappear slower than for the $L = 2D$ case but faster than for the wake behind a single cylinder in a constant flow. This difference between $L = 2D$ and $3D$ can be explained by the fact that the mean velocity mid-way between the cylinders accelerates to about 1.75 times the average velocity $\langle u \rangle$ across the tube bundle for the case $L = 2D$, but only to about 1.15 in the case $L = 3D$. In the latter case the mean strain is thus too weak to eliminate the wake.

For the case of the larger spacing our numerical results show that for the larger Reynolds numbers the effects of the upstream cylinder wake persist further than the distance L between the cylinders. Extrapolating from these results we estimate that the ‘wavelength’ L_C over which the effect of upwind wakes disappears is about equal to L when $L = 2D$, but is of order $2L$ when $L = 3D$. In other words the use of the ‘elemental’ cell as computation domain seems only allowed for $L \leq 2D$. The L_C/L seems to increase approximately in proportion to $2(L/D - 1)$ or L/D .

4.2. TURBULENT FLOW

Let us now consider the case with a Reynolds number, for which the flow is turbulent. An example is the experiments carried out by Simonin and Barcouda [20] at $Re = 18,000$. In this experiment $L = 45 \text{ mm}$ and $D = 21.7 \text{ mm}$ so that the ratio L/D is almost 2. We have simulated this case with the help of a DNS for a Reynolds number

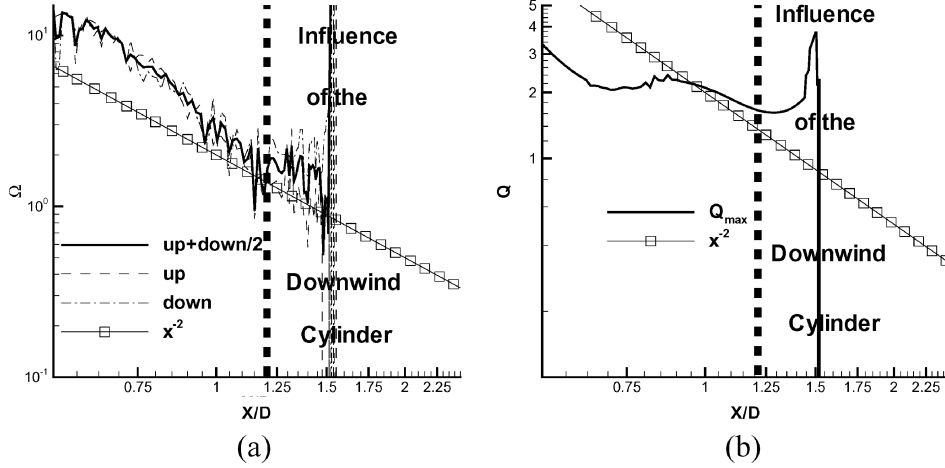


Figure 9. Turbulent wake in a tube bundle at $Re = 6000$. Compact spacing ($L \approx 2D$). (a) Vorticity maximum along x -axis; the lines indicated by up and down denote $\Omega_u(x)$ and $\Omega_d(x)$, respectively. (b) Volume flux along x -axis. The symbols \square in both figures denote the theoretical of the wake behaviour in a straining flow (following [5]) (note difference with high turbulence in Section 4.1).

of 6000. Although this Reynolds number is smaller than the experimental value, the flow is highly turbulent in both cases and therefore we expect the numerical simulation results to be comparable with the experimental data. In Moulinec *et al.* [17] we have presented statistics such as the mean velocity components and the Reynolds stresses and these have been found to agree well with the experimental data. We will not repeat this comparison here.

In Figure 9(a) we show for this simulation the maximum of vorticity $\Omega(x)$ and in Figure 9(b) the volume flux $Q(x)$ as a function of the x -coordinate behind the cylinder. In addition we have plotted the profiles of $\Omega_d(x)$ (indicated as down) and $\Omega_u(x)$ (indicated as up). In this turbulent flow we note that $\Omega(x)$ behaves approximately like x^{-2} (which has been predicted in section 3 for the case of highly turbulent flow). In contrast the volume flux $Q(x)$ does not vary significantly also in agreement with the prediction for highly turbulent flow. We thus find that in these strong turbulent flows the wake disappears over a short distance, as assumed in the investigation of Davidson *et al.* [6]. We conclude that the behaviour of the wake in this case is far from the features of highly strained turbulent flows studied by Hunt and Eames [5], but in fact is close to the behaviour expected for highly turbulent flows, for which wake dynamics is dominated by turbulent dispersion.

5. Diffusion of a Passive Scalar

So far we have looked at the statistics of the flow field. We now consider the diffusion of a passive scalar from a line source emitting within the tube bundle and in particular the effects of the general topology of the streamlines on the diffusion.

In addition to the computation of diffusion in the tube bundle we also consider the diffusion around a single cylinder in an infinite domain for the same Reynolds number. This has been computed with a mesh consisting of 120×80 cells. For the case of the tube bundle we consider the configurations $L = 2D$ and $3D$. To avoid the effects of boundary conditions on the scalar field, we have extended the computation domain to nine ‘elemental cells’ as shown in Figure 10(b) for $L = 2D$ case and in Figure 10(c) for the $L = 3D$ case. For the $L = 2D$ case the mesh consists of 144×144 grid points and for the $L = 3D$ of 240×240 grid points. The Reynolds number is equal to 150, for which we discussed in Section 4.1 that the flow is unsteady but effectively two-dimensional. The molecular diffusivity is taken equal to the kinematic viscosity, the Schmidt number being equal to 1. We refer to Figure 10 to illustrate the source positions.

In Figure 10(a) we show the average position of the concentration isoline $y_S(x)$, at which the concentration has dropped to about $1/10$ of the centreline value for

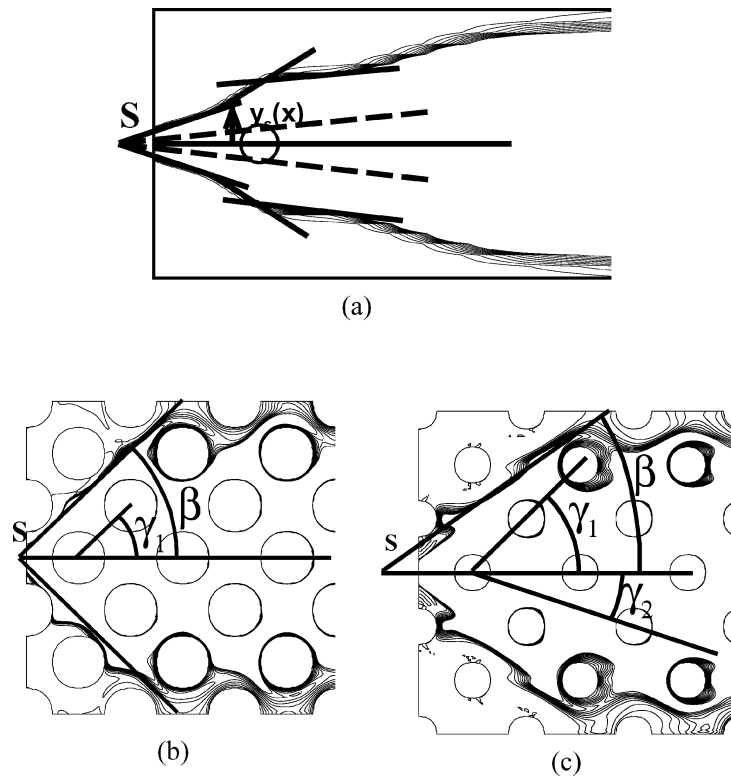


Figure 10. Diffusion of a passive scalar from a line source at $Re = 150$. (a) A single cylinder configuration (Note—denotes the much smaller plume in a uniform flow without an obstacle). (b) $L = 2D$ configuration with $\gamma_1 = 45^\circ$, where the initial dispersion angle is $\beta \approx \gamma_1 = 45^\circ$. (c) $L = 3D$ configuration with $\gamma_1 = 45^\circ$ and $\gamma_2 \approx 19^\circ$, where the initial dispersion angle is $\beta \approx 30^\circ$; note that $\gamma_2 < \beta < \gamma_1$.

the case of uniform flow past a single cylinder. Figure 10(a) shows that the $y_S(x)$ develops in distinct stages with a parabolic plume following $y_S \approx (Dx)^{1/2}$ far from the source.

In Figures 10 (b) and (c) we show the average position of the same concentration isoline $y_S(x)$, i.e. the isoline at which the concentration is about 1/10 of the centreline value, for the two cases of the tube bundle. The scalar primarily diffuses as a result of plume splitting as the streamlines pass either side along the downstream cylinders onto which the flow impinges. This is essentially the ‘topological effect’, pointed out earlier by Davidson *et al.* [6]. We can define two angles γ_1 and γ_2 , which characterize the geometry of the tubes in the tube bundle. The γ_1 is the angle between the x -axis and the diagonal of the ‘elemental cell’. The γ_2 is defined by the x -axis and the straight line meeting the origin and the point $(3/2 L, -1/2 L)$ (see Figure 10)(c). The ‘diffusion angle’ β , which is the angle between the initial part of the concentration isoline $y_S(x)$ and the x -axis, quantifies the lateral spread of the scalar. It follows from Figure 10(b) that for the case $L = 2D$ $\beta \approx 45^\circ$ or $\beta = \gamma_1$. For $L = 3D$ Figure 10(c) shows that $\beta \approx 30^\circ$ or $\gamma_2 < \beta < \gamma_1$. This result implies that the ‘diffusion angle’ β varies with the ratio L/D depending on the wake contraction induced by the proximity of the neighbouring cylinders. Further studies are needed to establish the general validity of this relationship between β and L/D .

6. Approximation to Flow in Tube Bundles

In Section 4 we have seen that our simulation results indicate that for the case $L \lesssim 2D$ the wake quickly disappears behind each cylinder for laminar flows. This result can also be extended to weakly turbulent flow when the effect of straining dominates the wake. In that case most of the flow is then rotation free and can thus be approximated by a potential flow. This allows us to use a much simpler and quicker method to estimate the flow field than by means of our direct numerical simulation.

The first step of this method is to get the potential flow solution for an infinite number of dipoles in a uniform parallel flow. The dipoles are aligned along a straight line, e.g. the x -axis, at a constant distance L . In Section 7 of the appendix we give the streamfunction for this case. Secondly, we generalize this result to a staggered set of rows of dipoles. The expression of the streamfunction for this latter case becomes

$$\Psi_{(\infty, \infty)}(x, y) = U \left(y - \frac{\pi D^2}{4L} \left(\sum_{k=-\infty}^{+\infty} \frac{\sin(2\pi \frac{y}{L})}{\cosh(2\pi(\frac{x}{L} - k)) - \cos(2\pi \frac{y}{L})} + \sum_{m=-\infty}^{+\infty} \frac{\sin(2\pi \frac{y+0.5L}{L})}{\cosh(2\pi(\frac{x+0.5L}{L} - k)) - \cos(2\pi \frac{y+0.5L}{L})} \right) \right) \quad (5)$$

where we refer to Appendix 7.1 for details of the computation.

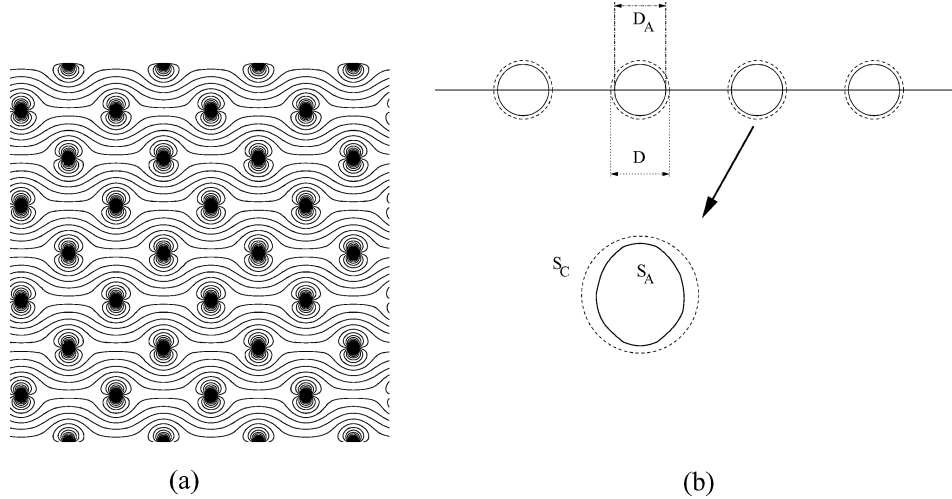


Figure 11. $L = 2D$. (a) Streamlines for the potential flow following from a staggered set of rows of dipoles in a uniform parallel flow. (b) Boundary of the distorted 'cylinder' S_A located along x -axis as an approximation to the exact cylinder S_C .

The resulting flow, of which a streamline pattern is illustrated in Figure 11(a), gives an approximation of the flow field in a staggered tube bundle. It is an approximation because the combination of dipoles does not represent exactly the flow around the cylinders of the tube bundle. This is shown in Figure 11(b) where we illustrate the surface given by the curve S_A centred on the x -axis, which is obtained from our dipole solution as the closed curve along which the flow is computed. It is clear that this surface is not exactly equal to a cylinder, i.e. to a circle as given by the curve S_C . The deviation, which depends on the proximity of the neighbouring cylinder or alternatively on L/D , is rather small as shown in Figure 11(b). We have investigated this deviation from an ideal circle for tube bundles with a spacing that varies between $1.5 < L/D < 3$. The results are plotted in Figure 12, where it is shown that the error defined as $\delta_D = (D - D_A)/D$, with D the diameter of the circle and D_A the diameter of the approximate body, behaves like $1/L^{1.75}$. An asymptotic estimate for $L \gg D$, suggests that this error δ_D should vary as $1/L^2$. Note that the magnitude of the error is already less than about 10% for $L/D > 2.5$.

For case of $L = 2D$ we have compared the result obtained with the potential flow method with the results obtained by our DNS computation at $Re = 6000$. For the DNS we have used a stretched mesh of $196 \times 196 \times 128$ cells. The calculation lasts for 1000 h on an ORIGIN3800 whereas the potential flow methods needs less than 1 min on the same computer. In Figure 13 we show the results for the streamlines in both cases. (Note that we have computed the DNS in an 'elemental cell' but in Figure 13(a) the domain has been extended to four 'elemental' cells by means of periodic continuation.) We find that the mean streamline pattern is qualitatively well predicted by the potential theory, especially in the acceleration part of the flow

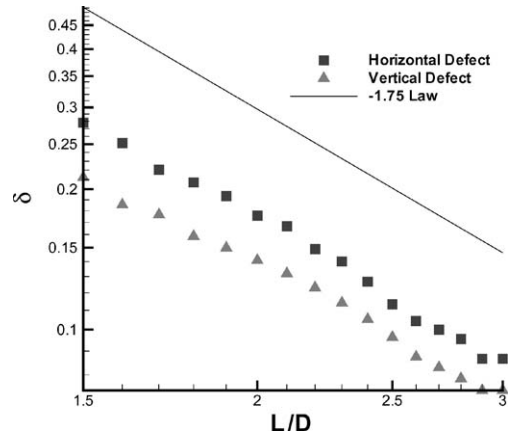


Figure 12. Shape distortion δ_A of a bundle of staggered cylinders as approximated by a series of dipoles as a function of L/D .

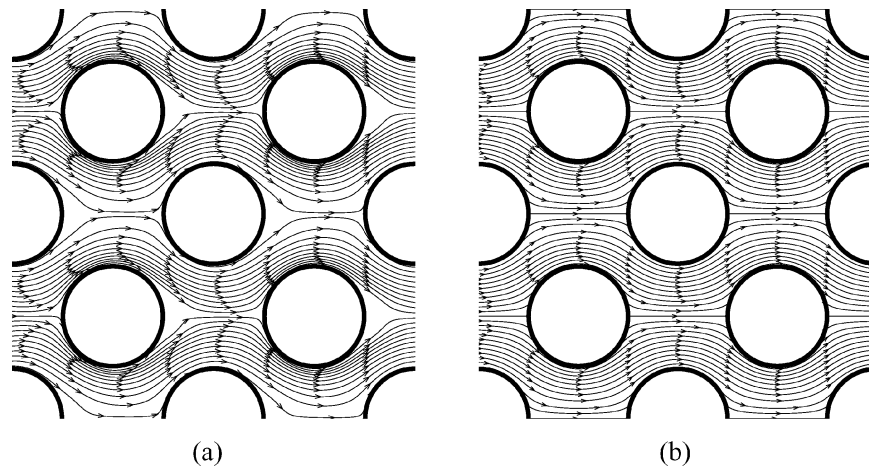


Figure 13. Streamline patterns in a tube bundle with $L = 2D$. (a) Mean streamlines in 3-D turbulent flow computed by means of DNS with the diagonal Cartesian method at $Re = 6000$. (b) Streamlines pattern obtained from potential flow method. Note the symmetry and the lack of any wakes.

where the distance between neighbouring cylinders is the smallest (i.e. the E and F zones in Figure 1). However, in the small recirculation zones behind the cylinders the inviscid model of course fails but this region is not of great significance for the computation of the dispersion problem.

7. Concluding Remarks

We have studied the flow through a packed array of cylindrical tubes in a staggered pattern. In particular we have studied the case for steady laminar flow at

moderate Reynolds number and for unsteady three-dimensional vortical flow at higher Reynolds number. We found that the recirculation length in the wake behind the cylinders of the tube bundle is much shorter than the recirculation length behind a single cylinder in a uniform flow in an unbounded domain. The explanation of this phenomenon is the vorticity cancellation due to the accelerated diffusion, which is caused by acceleration/deceleration of the flow between the cylinders in the tube bundle. This effect has not previously been identified as being important for tube bundle flows. The theory enables us to estimate the range of Reynolds numbers and of spacings of the tubes in the bundles where this phenomenon of wake disappearance occurs. As a result of this wake disappearance most of the flow domain can be approximated by a rotation-free flow and this means that we can use a potential flow model to approximate the flow in the tube bundle. Further studies are necessary to determine for which range of conditions this potential flow approximation is valid in two and three-dimensional geometries.

By means of DNS and the use of the diagonal Cartesian method we have also simulated the fully turbulent flow through tube bundle at a Reynolds number of 6000. Again the phenomenon of wake disappearance is found but in this case it is rather caused by the increased turbulent dispersion of the wake vorticity. The mean flow field and the turbulence in this flow geometry are strongly affected by the complex interaction of the flow around the cylinders. This has for instance a dominating influence on the dispersion of a scalar within the tube bundle flow which has been called ‘topological’ diffusion by Davidson *et al.* [6]. The dispersion normal to the flow is determined by the splitting of the streamlines as they impinge on the cylinders of the tube bundle. Molecular and turbulent diffusion are necessary for the process, but they only have weak effects on the magnitude of the spreading angle β . Further studies could provide more robust estimates of the effective diffusivities (and spreading angles) in different geometries.

The concepts identified in this study have some application to the even more complex problems of flows between moving and deforming bodies in engineering and environmental two-phase flow and perhaps for the case of randomly moving eddies in turbulent flows.

Appendix: Fast approximation to potential flow in tube bundles

FLOW AROUND AN INFINITY OF ALIGNED CYLINDERS

Potential flow around a single cylinder at the origin $(0, 0)$ of a two-dimensional coordinate system is represented by the complex potential of the combination of a uniform parallel flow with a dipole. It reads:

$$w(z) = Uz + \frac{D^2U}{4(z - z_{(0,0)})}$$

where D is the diameter of the cylinder and U the strength of the parallel flow.

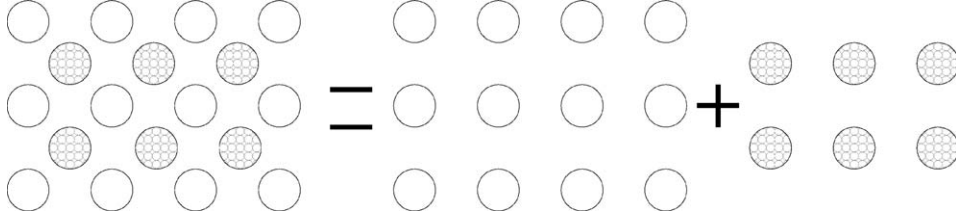


Figure 14. Staggered tube bundle seen as the sum of two aligned tube bundles.

Let us now consider the case of $2K + 1$ dipoles distributed with a constant distance L between neighbouring dipoles along a straight line, say the x -axis. The complex potential $w_{(K,0)}$ is obtained by summing the series of potentials as given above with

$$w_{(K,0)} = Uz + U \frac{D^2}{4} \sum_{k=-K}^{+K} \frac{1}{z - z_{(k,0)}}.$$

where $z_k = k \times L$. Note that in this approximation the stream surface S_A , which separates the dipole flow from the parallel flow is no longer exactly equal to a circular cylinder. The ‘error’ between has been analyzed in Section 6. When $K \rightarrow \infty$ the summation can be carried out exactly resulting in the following complex potential $w_{(\infty,0)}$:

$$w_{(\infty,0)} = U \left(z + \frac{i\pi D^2}{4L} \coth \left(i\pi \frac{z}{L} \right) \right) \quad (6)$$

The streamlines are obtained from the imaginary part of this potential and are given by:

$$\Psi_{(\infty,0)}(x, y) = U \left(y - \frac{\pi D^2}{4L} \frac{\sinh \left(\frac{2\pi y}{L} \right)}{\cosh \left(2\frac{\pi y}{L} \right) - \cos \left(2\frac{\pi x}{L} \right)} \right)$$

7.1. GENERALIZATION

The potential flow through a staggered array of tubes can now be approximated as the sum of two bundles of aligned tubes, the latter being shifted with respect to the former by the vector $(L/2, L/2)$ (see Figure 14). The total complex potential can then be obtained by summing (6) for each dipole row.

In the first bundle, the dipoles are centred in $z_{k,m} = (kL, mL)$ whereas in the second one they are located in $z_{k+1/2,m+1/2} = ((k+1/2)L, (m/2)L)$. Considering the first arrangement of dipoles, the following complex potential $w_{(K,M)}$ is calculated

with $(2K + 1) \times (2M + 1)$ dipoles

$$\begin{aligned}
 w_{(K,M)} &= U \frac{D^2}{4} \sum_{k=-K}^{+K} \sum_{m=-M}^{+M} \frac{1}{z - kL - imL} \\
 &= U \frac{D^2}{4} \sum_{k=-K}^{+K} \left(\frac{1}{z - kL} + \frac{2(\frac{z}{L} - k)}{L} \sum_{m=1}^{+M} \frac{1}{(\frac{z}{L} - k)^2 + m^2} \right) \quad (7) \\
 &= U \frac{D^2}{4} \sum_{k=-K}^{+K} \left(\frac{1}{L\xi} + \frac{2\xi}{L} \sum_{m=1}^{+M} \frac{1}{\xi^2 + m^2} \right)
 \end{aligned}$$

Here, $\xi = (z/L - k)$. From previous considerations, $\sum_{m=1}^{+M} 1/(\xi^2 + m^2)$ is defined for all ξ when $\xi \neq im$ and converges towards $\sum_{m=1}^{+\infty} 1/(\xi^2 + m^2) = -1/(2\xi^2) + \pi \coth(\pi\xi)/(2\xi)$. This leads to

$$\begin{aligned}
 w_{(K,\infty)} &= U \frac{D^2}{4} \sum_{k=-K}^{+K} \left(\frac{1}{L\xi} + \frac{2\xi}{L} \left(-\frac{1}{2\xi^2} + \frac{\pi \coth(\pi\xi)}{2\xi} \right) \right) \quad (8) \\
 &= U \frac{\pi D^2}{4L} \sum_{k=-K}^{+K} \coth \left(\pi \left(\frac{z}{L} - k \right) \right) = U \frac{\pi D^2}{4L} \sum_{k=-K}^{+K} s_k
 \end{aligned}$$

with $s_k = \coth(\pi(z/L - k)) = \coth(a + ib)$ where $a = \pi(x/L - k)$ and $b = \pi y/L$. The streamlines are then determined by the imaginary part of s_k , so that:

$$\begin{aligned}
 \Im(s_k) &= \Im(\coth(a + ib)) = \Im\left(\frac{\cosh(a) \cos(b) + i \sinh(a) \sin(b)}{\sinh(a) \cos(b) + i \cosh(a) \sin(b)}\right) \\
 &= -\frac{\sin(2b)}{\cosh(2a) - \cos(2b)}
 \end{aligned}$$

Finally,

$$\Im(w_{(K,\infty)}) = -U \frac{\pi D^2}{4L} \sum_{k=-K}^{+K} \frac{\sin(2\pi \frac{y}{L})}{\cosh(2\pi(\frac{x}{L} - k)) - \cos(2\pi \frac{y}{L})}.$$

The amplitude of this series is such that

$$\left| \frac{\sin(2\pi \frac{y}{L})}{\cosh(2\pi(\frac{x}{L} - k)) - \cos(2\pi \frac{y}{L})} \right| < \left| \frac{1}{\cosh(2\pi(\frac{x}{L} - k)) - \cos(2\pi \frac{y}{L})} \right|$$

and

$$\left| \frac{1}{\cosh(2\pi(\frac{x}{L} - k)) - \cos(2\pi \frac{y}{L})} \right| \sim e^{-2\pi k}$$

when $k \rightarrow \infty$ and

$$\left| \frac{1}{\cosh(2\pi(\frac{x}{L} - k)) - \cos(2\pi \frac{y}{L})} \right| \sim e^{2\pi k}$$

when $k \rightarrow -\infty$ this series therefore converges towards:

$$\Im(w_{(\infty, \infty)}) = -U \frac{\pi D^2}{4L} \sum_{k=-\infty}^{+\infty} \frac{\sin(2\pi \frac{y}{L})}{\cosh(2\pi(\frac{x}{L} - k)) - \cos(2\pi \frac{y}{L})}$$

To calculate the streamlines corresponding to the shifted set of dipoles, x is replaced by $x + L/2$ and y by $y + L/2$ in the previous equation. Based on these results the streamfunction for the staggered tube bundle becomes:

$$\Psi_{(\infty, \infty)}(x, y) = U \left(y - \frac{\pi D^2}{4L} \left(\sum_{k=-\infty}^{+\infty} \frac{\sin(2\pi \frac{y}{L})}{\cosh(2\pi(\frac{x}{L} - k)) - \cos(2\pi \frac{y}{L})} + \sum_{k=-\infty}^{+\infty} \frac{\sin(2\pi \frac{y+0.5L}{L})}{\cosh(2\pi(\frac{x+0.5L}{L} - k)) - \cos(2\pi \frac{y+0.5L}{L})} \right) \right)$$

The velocity components are easily derived from this streamfunction as follows:

$$u(x, y) = \frac{\partial \Psi_{(\infty, \infty)}}{\partial y}(x, y)$$

$$v(x, y) = -\frac{\partial \Psi_{(\infty, \infty)}}{\partial x}(x, y)$$

which leads to

$$u(x, y) = U \left(1 - \frac{\pi^2 D^2}{2L^2} \left(\sum_{k=-\infty}^{+\infty} \frac{\cos(2\pi \frac{y}{L}) \cosh(2\pi(\frac{x}{L} - k)) - 1}{(\cosh(2\pi(\frac{x}{L} - k)) - \cos(2\pi \frac{y}{L}))^2} + \sum_{k=-\infty}^{+\infty} \frac{\cos(2\pi \frac{y+0.5L}{L}) \cosh(2\pi(\frac{x+0.5L}{L} - k)) - 1}{(\cosh(2\pi(\frac{x+0.5L}{L} - k)) - \cos(2\pi \frac{y+0.5L}{L}))^2} \right) \right) \quad (9)$$

$$v(x, y) = -U \frac{\pi^2 D^2}{2L^2} \left(\sum_{k=-\infty}^{+\infty} \frac{\sin(2\pi \frac{y}{L}) \sinh(2\pi(\frac{x}{L} - k))}{(\cosh(2\pi(\frac{x}{L} - k)) - \cos(2\pi \frac{y}{L}))^2} + \sum_{k=-\infty}^{+\infty} \frac{\sin(2\pi \frac{y+0.5L}{L}) \sinh(2\pi(\frac{x+0.5L}{L} - k))}{(\cosh(2\pi(\frac{x+0.5L}{L} - k)) - \cos(2\pi \frac{y+0.5L}{L}))^2} \right)$$

Acknowledgments

We are grateful for conversations with I. Eames and S.E. Belcher. J.C.R. Hunt research is also supported by NERC at the Centre for Polar Observation and Modelling at U.C.L. Computer time was made available by the National Computing Facilities Foundation (NCF).

References

1. Planchard, J. and Ibnou-Zahir, M., Natural frequencies of tube bundle in an incompressible fluid. *Comp. Meth. Appl. Mech. Eng.* **41**(1) (1983) 47–68.

2. Schroder, K. and Gelbe, H., Two- and three-dimensional CFD-simulation of flow-induced vibration excitation in tube bundles. *Chem. Eng. Proc.* **38**(4–6) (1999) 621–629.
3. Longatte, E., Bendjeddou, Z. and Souli, M., Methods for numerical study of tube bundle vibrations in cross-flows. *J. Fluids Struct.* **8**(5) (2003) 513–528.
4. Belcher, S.E., Jerram, N. and Hunt, J.C.R., Adjustment of a turbulent boundary layer to a canopy of roughness elements. *J. Fluid Mech.* **488** (2003) 369–398.
5. Hunt, J.C.R. and Eames, I., The disappearance of laminar and turbulent wakes in complex flows. *J. Fluid Mech.* **457** (2002) 111–132.
6. Davidson, M.J., Mylne, K.R., Jones, C.D., Phillips, J.C., Perkins, R.J., Fung, J.C.H. and Hunt, J.C.R., Plume dispersion through large groups of obstacles: A field investigation. *Atmos. Environ.* **29** (1995) 3245–3256.
7. Elliot, C.J. and Townsend, A.A., The development of a turbulent wake in a distorting duct. *J. Fluid Mech.* **113** (1981) 433–467.
8. Keffer, J.F., Kawall, J.G., Hunt, J.C.R. and Maxey, M.R., The uniform distortion of thermal and velocity mixing layers. *J. Fluid Mech.* **86** (1978) 465–490.
9. Britter, R.E., Hunt, J.C.R. and Mumford, J.C., The distortion of turbulence by a circular cylinder. *J. Fluid Mech.* **92** (1979) 269–301.
10. Owen, P.R., Buffeting excitation of boiler tube vibration. *J. Mech. Eng. Sci.* **7** (1965) 431–439.
11. Benhamadouche, S. and Laurence, D., LES, coarse LES, and transient RANS comparisons on the flow across a tube bundle. *Int. J. Heat Fluid Flow* **24**(4) (2003) 470–479.
12. Rollet-Miet, P., Laurence, D. and Ferziger, J., LES and RANS of turbulent flow in tube bundles. *Int. J. Heat Fluid Flow* **20** (1999) 241–254.
13. Bouris, D. and Bergeles, G., Two-dimensional time dependent simulation of the subcritical flow in a staggered tube bundle using a subgrid scale model. *Int. J. Heat Fluid Flow* **20**(2) (1999) 105–114.
14. Hassan, Y.A. and Ibrahim, W.A., Turbulence prediction in two-dimensional bundle flows using large-eddy simulation. *Nucl. Techn.* **119** (1) (1997) 11–28.
15. Patankar, S.V., *Numerical Heat Transfer and Fluid Flows*. Hemisphere Publishing Co/McGraw-Hill Co, New York (1980).
16. Lin, W.L., Carlson, K.D. and Chen, C.J., Diagonal Cartesian method for modeling of incompressible flows over complex boundaries. *Num. Heat Transfer, Part B* **33** (1998) 181–213.
17. Moulinec, C., Pourquié, M.J.B.M., Boersma, B.J., Buchal, T. and Nieuwstadt, F.T.M., Direct numerical simulation of the flow in a tube bundle on a Cartesian mesh. *Int. J. Comp. Fluid Dyn.* **18** (1) (2004) 1–14.
18. Chorin, A.J., Numerical solution of the Navier-Stokes equations. *Math. Comp.* **22** (1968) 745–762.
19. Temam, R., Une méthode d’approximation de la solution des équations de Navier-Stokes. *Bull. Soc. Math. France* **8** (1968) 115–152.
20. Simonin, O. and Barcouda, M., Measurements of fully developed turbulent flow across tube bundle. In: *3ème Conférence Internationale sur les Applications de l’Anémométrie Laser à la Mécanique des Fluides* (1986).
21. Meyer, K.E., Experimental and numerical investigation of turbulent flow and heat transfer in staggered tube bundles. Ph.D. Thesis, Technical University of Denmark, Lyngby (1994) .
22. Kravchenko, A.G. and Moin, P., Numerical studies of flow over a circular cylinder at $Re_D = 3900$. *Phys. Fluids* **12** (2000) 403–417.